



# Enantioselective hydrogenation of 1-phenyl-1,2-propanedione on immobilised cinchonidine-TiO<sub>2</sub> catalysts



Cristian H. Campos<sup>a</sup>, Cecilia C. Torres<sup>a</sup>, Ana B. Dongil<sup>a</sup>, Doris Ruiz<sup>a</sup>, José L.G. Fierro<sup>b</sup>, Patricio Reyes<sup>a,\*</sup>

<sup>a</sup> Edmundo Larenas 129/Departamento de Fisicoquímica, Facultad de Ciencias Químicas, Universidad de Concepción, Concepción, Chile

<sup>b</sup> Instituto de Catálisis y Petroleoquímica, CSIC, Marie Curie 2, Cantoblanco 28049, Madrid, Spain

## ARTICLE INFO

### Article history:

Received 14 November 2013

Received in revised form 19 April 2014

Accepted 29 April 2014

Available online 12 June 2014

### Keywords:

TiO<sub>2</sub> catalysts

Immobilised cinchonidine

1-Phenyl-propane-1,2-dione

Enantioselective hydrogenation

## ABSTRACT

The enantioselective hydrogenation of 1-phenyl-1,2-propanedione (PPD) was investigated using cinchonidine-immobilised Pt/TiO<sub>2</sub> catalysts. Prior to metal deposition, TiO<sub>2</sub> was chirally modified by the direct anchoring of cinchonidine (CD) using trimethoxysilane as coupling agent (TMS-CD). The catalysts were prepared using a high H<sub>2</sub> pressure reduction-deposition method and were characterised by elemental analysis (C, H and N), TG, DRIFT, <sup>13</sup>C and <sup>29</sup>Si solid-state NMR, N<sub>2</sub> adsorption-desorption isotherms, XRD, XPS and HR-TEM. The catalytic activity was evaluated in a batch reactor at 298 K and 40 bar using cyclohexane as solvent with various cinchonidine concentrations. The results indicate that the enantioselectivity was sensitive to the CD surface concentration and the enantiomeric excess of the target product, 1-R-phenyl-1-hydroxy-2-propanone, was in the range of 25–51%. The best catalyst was the one supported on TiO<sub>2</sub> with a nominal content of 10 wt% TMS-CD. The effect of the H<sub>2</sub> pressure, the concentration of substrate, solvent and recyclability of the catalyst were studied. The results obtained confirmed that the variation of reaction conditions affects both the activity and enantioselectivity due to the substrate adsorption on the metal active sites. Concerning the solvent effect, the enantiomeric excess decreased non-linearly upon increasing the solvent dielectric constant; this was attributed to the interactions between solvents and TMS-CD on the surface. In the catalyst recycling studies, the enantiomeric excess decreased up to 40% after the 3rd reuse. The drop of activity and enantiomeric excess was attributed to the hydrogenation of the immobilised CD.

© 2014 Elsevier B.V. All rights reserved.

## 1. Introduction

Asymmetric catalysis has become a challenging subject in the field of organic synthesis and catalysis over the past three decades, both from the theoretical and practical points of view [1–3]. Among the numerous enantioselective heterogeneous reactions, the Pt/cinchona-catalysed hydrogenation of  $\alpha$ -ketoesters is one of the few successful examples with more than 95% enantiomeric excess (e.e.) under favourable reaction conditions [4]. Another typical reaction is the hydrogenation of  $\alpha$ -diketones, which was first reported by Vermeer et al. in 1993 [5]. Due to the conjugated keto groups of the reactant, the hydrogenation consists of two consecutive steps. 1-Phenyl-1,2-propanedione (PPD) is a suitable molecule to investigate the enantioselective hydrogenation of conjugated carbonyl bonds [6–12]. It contains a phenyl ring and two carbonyl groups. Under the reaction conditions, in the presence of CD, the

main product is (R)-1-hydroxy-1-phenylpropanone, an important intermediate in the synthesis of drugs [13].

The commercial application of these systems requires an effective method of catalyst recovery and re-use because of economic and environmental concerns. Several methods for the recycling of chiral catalysts have been described [14–18] and a number of reactions have been conducted with this new type of catalysts, especially since the successful immobilisation of CD [19–21]. In previous papers, we investigated the enantioselective hydrogenation of PPD over two types of CD immobilisation: (1) using it as a stabiliser on Pt nanoclusters supported on SiO<sub>2</sub> [22,23], and (2) anchoring it on SiO<sub>2</sub> and  $\gamma$ -Al<sub>2</sub>O<sub>3</sub> oxides surfaces [20,21]. The catalysts not only exhibited similar enantioselectivity (i.e., 50% enantiomeric excess for the hydrogenation of PPD) but also exhibited novel catalytic properties, i.e., high regioselectivity to C=O adjacent to phenyl groups, which differs from their conventional heterogeneous counterparts.

As an extension of these previous studies, we describe in this paper the catalytic performance of Pt supported on CD modified TiO<sub>2</sub>-anatase in the enantioselective hydrogenation of PPD. We

\* Corresponding author.

E-mail addresses: [ccampose@udec.cl](mailto:ccampose@udec.cl) (C.H. Campos), [preyes@udec.cl](mailto:preyes@udec.cl) (P. Reyes).

attempt to show some insight on the role of the support on activity and selectivity. The study is focused on the direct tethering of modified CD molecules on pure anatase  $\text{TiO}_2$  using CD functionalised with trimethoxysilane (TMS-CD). The active phase deposition was performed using  $\text{H}_2\text{PtCl}_6$  as a precursor at high  $\text{H}_2$  pressure and room temperature. Some important reaction parameters, such as the surface modifier concentration, PPD concentration,  $\text{H}_2$  pressure and solvent, which have been less studied in the literature, were investigated in detail to optimise the enantioselectivity as well as the activity.

## 2. Experimental

### 2.1. Materials

All air-sensitive reactions were performed under an inert atmosphere (Ar) in a Schlenk flask. Tetrahydrofuran (THF, Merck<sup>®</sup>) and toluene (Merck<sup>®</sup>) were dried in metallic sodium/benzophenone; triethylamine (TEA, Aldrich<sup>®</sup>) was distilled at reduced pressure prior to use. Cinchonidine (96% Aldrich<sup>®</sup>), trimethylchlorosilane (TMCS 98%, Merck<sup>®</sup>), trimethoxysilane (TMS 98%, Merck<sup>®</sup>), platinum cyclooctadienyl (II) chloride ( $\text{Pt}(\text{COD})\text{Cl}_2$ , Aldrich<sup>®</sup>), anhydrous sodium sulphate ( $\text{Na}_2\text{SO}_4$ , Merck<sup>®</sup>), titanium(IV) oxide,  $\text{TiO}_2$ -anatase (99% AlfaAesar<sup>®</sup>),  $\text{H}_2\text{PtCl}_6 \cdot 6\text{H}_2\text{O}$  (40% Pt, Merck<sup>®</sup>), NaOH (Merck<sup>®</sup>), and the solvents (cyclohexane, ethanol, ethyl acetate, Merck<sup>®</sup>) were used as received.

### 2.2. Activation of $\text{TiO}_2$

$\text{TiO}_2$  activation was performed primarily to increase the surface concentration of Ti-OH groups because they are responsible for

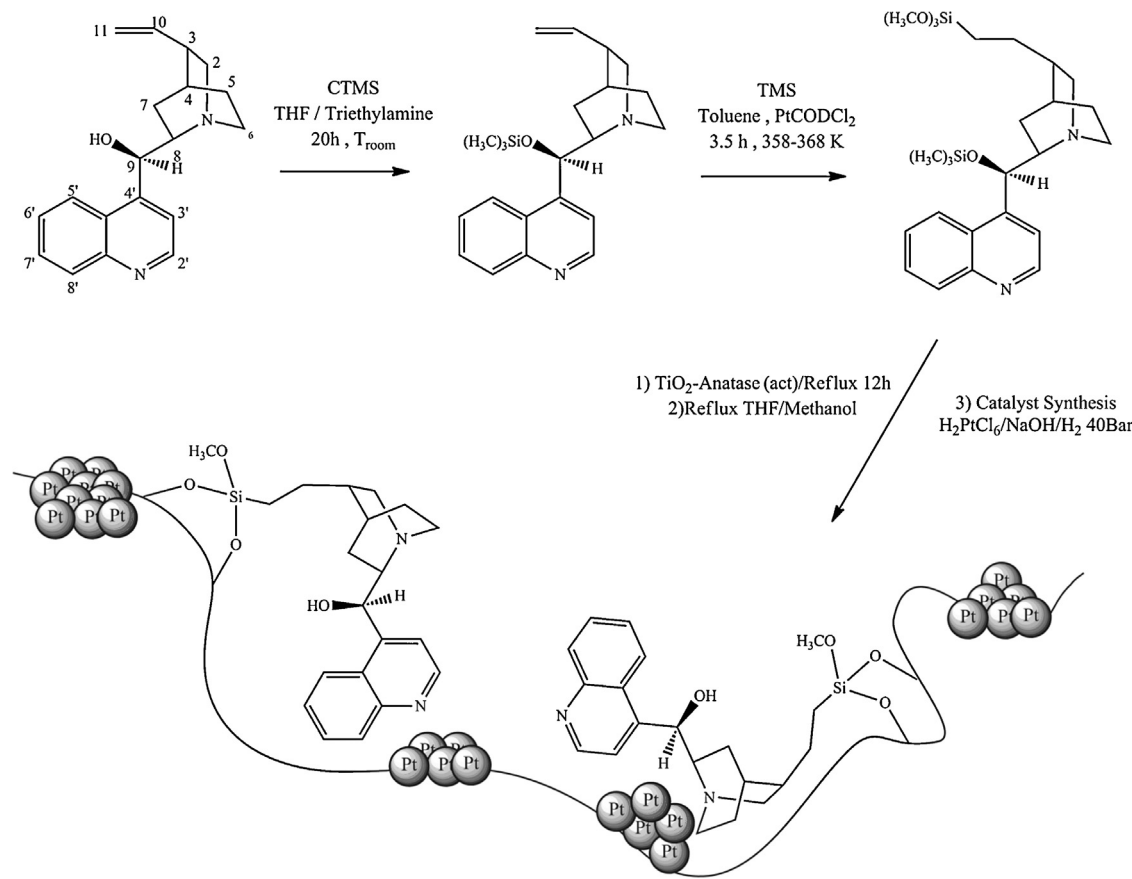
the immobilisation of TMS-CD, as reported in our own previous works [20,21]. Activation of the  $\text{TiO}_2$  surface was performed in a round-bottom flask in which 3.0 g of  $\text{TiO}_2$  was mixed with 24 mL of 1,4-dioxane and 3 mL of aqueous solution of 3.1 mol L<sup>-1</sup> HCl. This system was stirred for 30 min at 353 K, filtered, and dried under vacuum (lower than 10<sup>-1</sup> mbar) for 4 h at 393 K.

### 2.3. Preparation of modified CD

The modification of CD and the subsequent later hydroxylation were performed as reported in our previous works [20,21]. Briefly, an ice-cooled solution of CD in THF containing TEA was added dropwise to the TMCS. The reaction mixture was stirred for 20 h at room temperature and then for 2 h at 333 K. The product was extracted with chloroform and washed with water. The obtained product was hydroxylated with the  $\text{Pt}(\text{COD})\text{Cl}_2$  catalyst precursor and TMS (TMS/catalyst = 120, mole ratio) at 313 K using toluene as the solvent. The reaction mixture was stirred for 5 h at 363 K under a N<sub>2</sub> atmosphere. Purification was performed by flash chromatography (hexane-acetone-TEA = 40:18:1).

### 2.4. Synthesis of modified $\text{TiO}_2$

Five supports were prepared with different amounts of CD (1, 5, 10, 15, and 20 wt%), simulating the CD fractions that are added in traditional systems. A 2.0 g sample of activated  $\text{TiO}_2$  and the appropriate amount of TMS-CD in toluene were added into a round-bottom flask, and the volume of the system was then brought to 50 mL with solvent (see Scheme 1). The reaction was refluxed for 12 h and later filtered and washed twice with 40 mL toluene and 20 mL chloroform. The solid was dried in a furnace for 1 h at 353 K.



**Scheme 1.** Synthetic route for CD modification and catalyst preparation.

Subsequently, the solid was treated by refluxing in a mixture of methanol/THF for 20 h and was then washed with 100 mL of n-pentane. Finally, the solids were dried under vacuum for 4 h at 393 K. All the samples of the modified supports were denoted as TiCD[x], where [x] is the nominal TMS-CD wt% and, in the case of 0, corresponds to TiO<sub>2</sub>-activated support.

## 2.5. Catalyst preparation

The catalysts (1.0 g) were prepared to obtain 1 wt% Pt loading using the five modified supports and activated TiO<sub>2</sub>. These were labelled as 1%Pt/TiCD[x], with [x] = 1–20. The methodology is similar to that reported in our previous work [21]. The support was dispersed in 50 mL of deionised water in a Teflon container, and the appropriate amount of H<sub>2</sub>PtCl<sub>6</sub>·6H<sub>2</sub>O was added. After 1 h, 0.5 mol L<sup>-1</sup> NaOH was added (OH<sup>-</sup>Pt = 6) and sealed in a stainless steel batch reactor. The pressure was adjusted to 40 bar H<sub>2</sub> for 2 h under constant magnetic stirring, obtaining the reduced supported metal. Then, the solid was filtered off and washed to constant values of pH and conductivity. Finally, it was dried in a vacuum oven at 373 K for 1 h and stored in a desiccator under N<sub>2</sub> atmosphere prior to the catalytic test.

## 2.6. Catalyst characterisation

Elemental analyses of C, H, and N were performed on a LECO CHNS-932 analyser. TG studies were conducted in a Mettler Toledo Thermogravimetric TGA/SDTA 851 using an O<sub>2</sub> flow of 25 mL min<sup>-1</sup> and a heating rate of 1 K min<sup>-1</sup> from 298 to 1000 K. NMR spectra for <sup>1</sup>H and <sup>13</sup>C{<sup>1</sup>H} were obtained on a Bruker AMX-300 spectrometer (300 MHz for <sup>1</sup>H, 75 MHz for <sup>13</sup>C) using trimethylsilane as an internal standard. The results obtained from the NMR of <sup>1</sup>H and <sup>13</sup>C were compared with those reported by Leino et al. [24,25]. Solid-state <sup>13</sup>C and <sup>29</sup>Si CP NMR spectra were recorded at 100.6 MHz and 79.49 MHz, respectively, using a Bruker AV 400 WB spectrometer. Diffuse reflectance infrared Fourier transform (DRIFTS) spectra were performed on a JASCO FT/IR-6300 fitted with an MCT-A detector and a KBr beamsplitter within the range of 4000–650 cm<sup>-1</sup>. Approximately 0.020 g of the sample was loaded into a diffuse reflectance (DRIFTS) reaction cell provided by Harrick (Praying Mantis model). Before any measurements were performed, the sample was heated for 1 h at 423 K in He flowing at 30 mL min<sup>-1</sup> and then cooled to room temperature. For all the measurements, spectra were a composite of 64 scans with a resolution of 4 cm<sup>-1</sup>. Prior to the run, backgrounds were collected by flowing He (at 30 mL min<sup>-1</sup>) at the respective reaction temperature. XRD patterns were recorded in a RigakuD/max-2500 diffractometer with Cu K $\alpha$  radiation at 40 kV and 100 mA. N<sub>2</sub> adsorption–desorption isotherms at 77 K were performed in a Micromeritics ASAP 2010 apparatus. Specific surface areas were determined by the BET (Brunauer–Emmett–Teller) equation, using adsorption data in the relative pressure range of 0.05–0.3, and pore-size distributions were estimated using the BJH method. TEM images of the catalysts were obtained using a Philips electron microscope CM200 with an energy dispersive analyser and digital camera coupled to a high speed TVIPS FastScan F-114 model of 1024 × 1024 pixels and 12 bits and a scanning electronic microscope JEOL JSM-6380 LV with a high resolution of 3.0 nm. The samples for analysis were prepared by dispersion in ethanol/H<sub>2</sub>O (1:1) and were deposited on a holey carbon/Cu grid (300 Mesh). Up to 300 individual metal particles were counted for each catalyst, and the surface area-weighted mean Pt diameter ( $d_p$ ) was calculated from:

$$d_p = \frac{\sum_i n_i d_i^3}{\sum_i n_i d_i^2}$$

where  $n_i$  is the number of particles of diameter  $d_i$ . The size limit for the detection of Pt particles on samples was ca. 0.1 nm.

Photoelectron spectra (XPS) were recorded using a VG Escalab 200 R spectrometer equipped with a hemispherical analyser and using non-monochromatic Mg K $\alpha$  X-ray radiation ( $h\nu = 1253.6$  eV). The binding energies (BE) were calculated with respect to the C-component of the C1s peak fixed at 284.8 eV. Data analysis was performed with the “XPS Peak” software. The peaks were decomposed into a sum of Gaussian/Lorentzian (G/L = 90/10) after the subtraction of a Shirley type baseline. The surface Pt/Ti and N/Ti atomic ratios were estimated from the integrated intensities of the Pt 4f, Ti 2p, C 1s, and N 1s lines after background subtraction and were corrected by the atomic sensitivity factors [26].

## 2.7. Catalytic activity

The catalytic assays of PPD hydrogenation were performed in a stainless steel (100 mL) Parr-type batch reactor at a concentration of 0.01 mol L<sup>-1</sup> of substrate using cyclohexane (25 mL) as solvent and stirring at 700 rpm under 40 bar of H<sub>2</sub> pressure. All catalytic runs were conducted in the absence of external mass transfer limitations. The catalysts were in the form of fine powders (>30  $\mu$ m), assuming a negligible effect of pore diffusion limitations. In the catalyst mass studies, the (PPD/Pt) molar ratio was varied, the concentration of PPD was kept constant and the mass of the catalyst was modified. No important differences in the initial reaction rates were noted upon varying the catalyst mass in the 0.01–0.07 g range because the reaction rate was proportional to the catalyst mass. This indicated that gas–liquid and liquid–solid external mass transfer limitations were absent [9,27]. The pseudo-kinetic constants ( $k$ ) were calculated using a pseudo-first-order kinetic model for a batch reactor in similar conditions, as was reported by Toukoniitty et al. [10]. In our case, only 4 hydrogenation products were detected, as shown in Scheme 2.

Reactants and products were analysed by gas chromatography and mass spectrometry using a GC-MS device (Shimadzu GCMS-QP5050) with a 30 m chiral  $\beta$ -Dex 225 column (Supelco®) and helium as the carrier gas. The recycling assays were performed by filtering the catalyst from the reaction medium. The filtered catalyst was washed three times consecutively with chloroform to clean the surface and was then dried at 373 K for 24 h.

In relation to the selectivity of the catalysts, enantiomeric excess and regioselectivity have been defined as:

$$\text{ee}_{Cx}(\%) = \frac{[R]_x - [S]_x}{[R]_x + [S]_x} \times 100 \quad \text{and} \quad rs = \frac{[R_{C1}] + [S_{C1}]}{[R_{C2}] + [S_{C2}]}$$

where [R] and [S] correspond to the concentration of the respective enantiomers,  $x$  is the number of the carbonyl group, and in the case of rs, of the alcohols of the different carbonyl groups.

## 3. Results and discussion

### 3.1. Support synthesis and characterisation

**Table 1** summarises the elemental analysis of the supports. The total content of TMS-CD anchored on the surface was lower than the nominal content, and the effect was more pronounced upon increasing the nominal content of the inducer. The calculations were based on the N(%) because it is the only vector of the real TMS-CD content anchored on TiO<sub>2</sub>, as reported in our previous works [20,21]. These observations can be explained in terms of the nature of the Ti-OH groups developed on the activated TiO<sub>2</sub> surface and diffusion phenomena, respectively. The 1,4-dioxane/HCl-treatment increases the amount of hydroxyls on the titanium surface. These Ti-OH groups exhibit different surface structural arrangements, with different surface reactivity: (1)

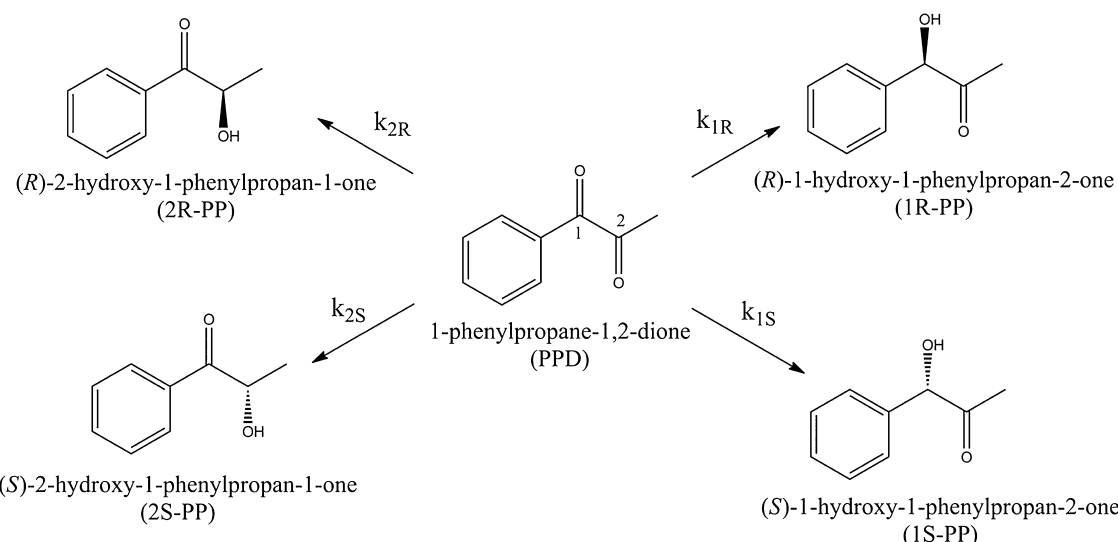


**Table 1**  
Elemental analysis (at%) and TMS-CD content determined by EA and TGA of the synthesised supports.

| Sample   | C(%) | H(%) | N(%) | TMS-CD (wt%) |     | Yield <sup>a</sup> (%) |
|----------|------|------|------|--------------|-----|------------------------|
|          |      |      |      | EA           | TGA |                        |
| TiCD(1)  | 1.69 | 0.63 | 0.07 | 1.0          | 6.0 | 99.3                   |
| TiCD(5)  | 2.71 | 0.84 | 0.25 | 3.5          | 7.4 | 70.0                   |
| TiCD(10) | 3.43 | 0.95 | 0.42 | 6.0          | 8.4 | 60.0                   |
| TiCD(15) | 4.06 | 1.03 | 0.54 | 7.8          | 9.0 | 51.4                   |
| TiCD(20) | 4.72 | 1.01 | 0.62 | 8.8          | 9.2 | 43.9                   |

<sup>a</sup> Yield of elemental analysis:  $(\text{TMS-CD}_{\text{Real}}/\text{TMS-CD}_{\text{Nominal}}) \times 100\%$ .

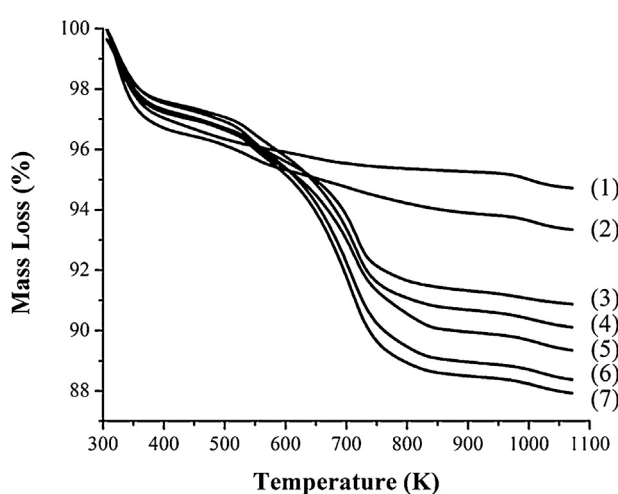
hydroxyls groups, with different acid–base character, that can form hydrogen bonds from multilayer arrangements; and (2) free hydroxyl groups characterised by lower coordination interactions, such as that located at the corners and defects on the catalyst surface, usually considered to be the most basic ones [28]. In our system, the first arrangement would decrease the ability to form Ti–O–Si bond during the TMS-CD immobilisation.

Fig. 1 displays the thermogravimetric mass changes for the different materials. For  $\text{TiO}_2$ , a mass loss of 2 wt% in the 400–1000 K

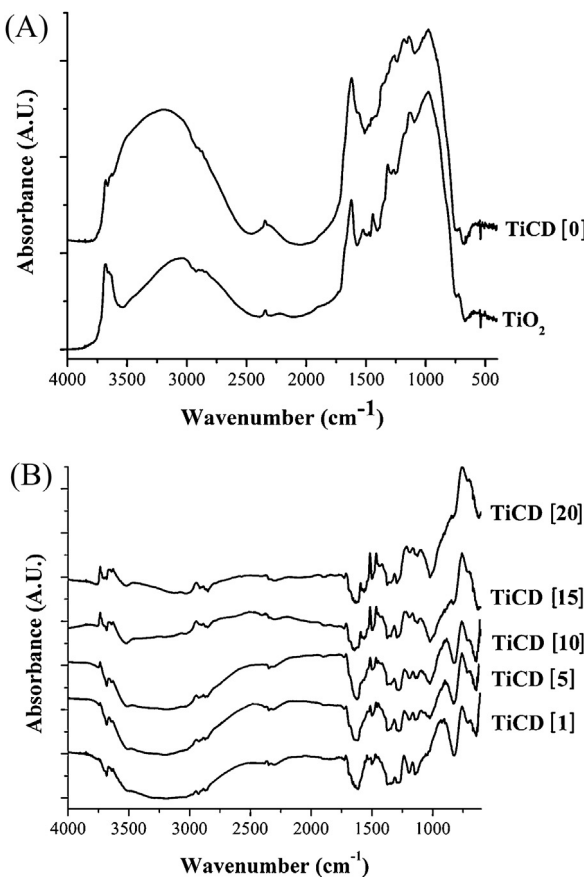
range, which corresponds to the dehydroxylation and accounts for  $1.2 \text{ mmol}_{\text{OH}} \text{ g}^{-1}$ . After the activation treatment, the TiCD(0) displayed a new slope in the range 400–1000 K corresponding to 4 wt% mass, approximately  $2.4 \text{ mmol}_{\text{OH}} \text{ g}^{-1}$ . The supports modified with TMS-CD showed three steps of mass losses in the ranges 298–350 K, 550 K and 650–750 K. The first mass loss corresponds to desorption of the water absorbed when the samples were exposed to the atmosphere prior to TG measurements. The second mass change is associated to the degradation of alkyl chains and the third corresponds to the quinoline aromatic ring oxidation [20]. The TMS-CD content obtained by TGA shows an excess with respect to the EA, as shown in Table 1. For the TiCD[x] supports, the TMS-CD immobilisation process (the reflux treatment with toluene and  $\text{THF}/\text{CH}_3\text{OH}$  and washing with n-pentane) can be attributed to strong solvent adsorption.

Fig. 2 shows the DRIFT spectra of the  $\text{TiO}_2$ -anatase and the modified supports. The parent  $\text{TiO}_2$  showed intense bands at 3674, 3630, and  $1624 \text{ cm}^{-1}$ , corresponding to vibrations of hydroxyl groups on the surface of  $\text{TiO}_2$ , and at  $1624 \text{ cm}^{-1}$ , due to the bending mode of molecularly adsorbed water molecules. After the activation treatment, TiCD(0) displayed a broad band between 4000 and  $3000 \text{ cm}^{-1}$  due to the increase of the population of hydroxyl groups, as shown in Fig. 2(a). The intensity and width of this band can be explained by the different type of Ti–OH groups on the surface, in agreement with the TG results. With respect to the spectra profiles in Fig. 2(b), TiCD[x] with  $[x] \neq 0$  displayed bands in the range  $2956$ – $2863 \text{ cm}^{-1}$  and  $1540$ – $1200 \text{ cm}^{-1}$ . The first is associated with the C–H stretching vibrations of the quinuclidine heterocyclic ring, whereas in the second, the fingerprint bands of the TMS-CD are expected to occur. Upon increasing the nominal content of TMS-CD, the intensity of these bands increased, whereas the intensity of the band in the  $4000$ – $3000 \text{ cm}^{-1}$  range follows the opposite trend. Another band was detected at  $1115 \text{ cm}^{-1}$ , which can be assigned to the stretching vibration of the Ti–O–Si<sub>organic</sub> bonds, and it would confirm the covalent immobilisation of TMS-CD on  $\text{TiO}_2$ .

To support the DRIFT results,  $^{13}\text{C}$  and  $^{29}\text{Si}$  CP/MAS-NMR spectra were recorded and are displayed in Fig. 3(a) and (b), respectively.  $^{13}\text{C}$  NMR spectra displayed, for all the supports TiCD[x] with  $[x] \square 1$ , resonances in the range of 24–67 ppm, which are characteristic of the quinuclidine moiety of TMS-CD [19–21]. Additional resonances at 118, 128.8 and 137.7 ppm were also observed, which correspond to the aromatic quinoline ring. In our previous works, an unusual  $^{13}\text{C}$  signal was observed at ca.  $-2.0 \text{ ppm}$ , due to the Si–CH<sub>3</sub> moiety, but it was not detected in the TiCD[x] support. This could be



**Fig. 1.** TG curves for the synthesis of supports. Conditions:  $\text{O}_2$  atmosphere to  $25 \text{ mL min}^{-1}$  flow and temperatures in the range of 298–1000 K. (1)  $\text{TiO}_2$ ; (2) TiCD[0]; (3) TiCD[1]; (4) TiCD[5]; (5) TiCD[10]; (6) TiCD[15]; (7) TiCD[20].



**Fig. 2.** DRIFT of the supports modified with TMS-CD. (A)  $\text{TiO}_2$ -anatase and  $\text{TiO}_2$ -activated support; (B)  $\text{TiCD}[x]$  supports where the  $\text{TiO}_2$ -activated support spectra was subtracted.

explained by the acid–base nature of the  $\text{Ti}-\text{OH}$  groups of the prepared support.

Fig. 3(b) shows the  $^{29}\text{Si}$  NMR for the  $\text{TiCD}(20)$ . This technique is very sensitive to Si-atoms near  $-\text{OH}$  and/or  $-\text{OR}$  groups, and it is the standard characterisation method for silicate materials. Two signal types can be distinguished with this technique. The first type of signal arises from the anchored TMS-CD species that form bonds with the support/silicon alkoxides ( $-45$  to  $60$  ppm denominated  $T^x$  signal, where  $x = 1, 2$ , or  $3$ ). The second signal type corresponds to siloxane/silane ( $-90$  to  $-115$  ppm denominated  $Q^y$  signals, where  $y = 2, 3$  or  $4$ ) that remain after the anchoring process. Because this support possesses the major TMS-CD content on the surface, the characteristic anchoring signals of the  $T^2$  and  $T^3$  type at  $-50$  and  $-80$  ppm were detected, in agreement with the results we reported previously [20,21]. For the  $Q$  signals, two silanols were detected, with a similar intensity between the  $T$  and  $Q$  signals. The two  $Q^3$  signals, which were attributed to free silanol groups, occurred at  $-101.5$  and  $-108.3$  ppm in different chemical environments.  $\text{TiO}_2$  is an amphoteric metal oxide with acid–base pairs of  $\text{Ti}^{4+}$  (Lewis acid) and  $\text{O}^{2-}$  (Lewis base) ions on its surface [28]. These acid–base pairs can interact with the remaining free silanol groups and cause the signals that exhibit different chemical shifts. This interaction is very strong. Consequently, we assumed that the resonance at  $-108.3$  ppm corresponds to free silanol groups, whereas the resonance at  $-101.5$  ppm can be assigned to the strong interaction with the inorganic phase. The characteristic resonance of an Si atom coordinated with one O atom from the  $\text{TiO}_2$  network ( $13$  ppm) was not observed (Si impurities). This result is in agreement with the  $^{13}\text{C}$  NMR characterisation and it would confirm the

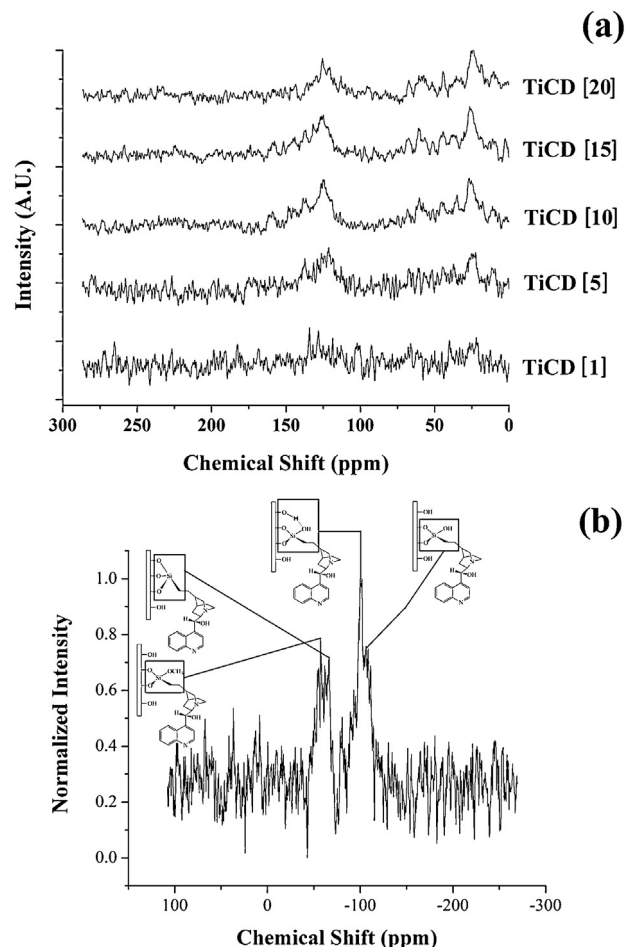


**Fig. 3.** Solid state CP-MAS NMR of the supports modified with TMS-CD. (a)  $^{13}\text{C}$  for  $\text{TiCD}[x]$  and (b)  $^{29}\text{Si}$  for  $\text{TiCD}[20]$ .

absence of impurities. The above characterisation results confirm the proposed reaction suggested in Scheme 1.

### 3.2. Catalyst synthesis and characterisation

Table 2 summarises the elemental analysis of the catalysts and the most relevant physicochemical properties. It can be observed that the TMS-CD content decreased with respect to the metal free counterparts in Table 1. This is due to a slight leaching of the inducer under the preparation conditions, as discussed in previous work [20,21]. The values of the BET surface areas of pure  $\text{TiO}_2$ -anatase and  $\text{TiCD}[x]$  are also summarised in Table 2. All the samples show type IV isotherms with type H4 hysteresis loops, according to IUPAC classification, corresponding to slit-shaped pores [29]. The surface area of pure  $\text{TiO}_2$ -anatase was  $142 \text{ m}^2 \text{ g}^{-1}$ , which is larger than the  $\text{TiCD}[x]$  samples. All of them displayed bi-modal pore-size distributions. This information allows us to infer that as the TMS-CD content increased, the porosity and surface area were influenced by the anchoring of TMS-CD species on the surface.

Fig. 4 shows the XRD patterns of the 1%Pt/ $\text{TiCD}[x]$  powdered samples. The dominant peaks at  $2\theta$   $25.4^\circ$ ,  $37.9^\circ$  and  $48.2^\circ$ , which represent the (101), (004) and (200) planes, respectively, correspond to the anatase phase. The absence of diffraction lines at  $27.4^\circ$ ,  $36.2^\circ$  and  $41.2^\circ$ , which correspond to the rutile phase, confirm that the prepared Pt/ $\text{TiCD}[x]$  powders consist of pure anatase. HR-TEM was used to estimate the average Pt particle size, and some images are shown in Fig. 5, where the dark spots on the large  $\text{TiO}_2$

**Table 2**

Elemental analysis and physicochemical properties:  $S_{\text{BET}}$ , pore diameter and metallic nanoparticles diameter of 1%Pt/TiCD( $x$ ) catalysts.

| Sample                    | N (at%) | TMS-CD (wt%) | CD maintained <sup>a</sup> (%) | $S_{\text{BET}}$ ( $\text{m}^2 \text{ g}^{-1}$ ) | Pore diameter (nm) |       | $d_p$ HR-TEM (nm) |
|---------------------------|---------|--------------|--------------------------------|--|--------------------|-------|-------------------|
|                           |         |              |                                |  | $d_1$              | $d_2$ |                   |
| TiO <sub>2</sub> -anatase | –       | –            | –                              | 142  | 4.1                | 9.8   | –                 |
| 1%Pt/TiCD(0)              | –       | –            | –                              | 139  | 4.0                | 9.5   | 2.6               |
| 1%Pt/TiCD(1)              | 0.07    | 0.9          | 93.5                           | 139  | 3.9                | 9.4   | 2.1               |
| 1%Pt/TiCD(5)              | 0.14    | 2.0          | 57.1                           | 134  | 3.6                | 9.2   | 2.5               |
| 1%Pt/TiCD(10)             | 0.22    | 3.2          | 52.4                           | 131  | 3.6                | 9.1   | 2.6               |
| 1%Pt/TiCD(15)             | 0.30    | 4.3          | 55.6                           | 123  | 3.3                | 9.0   | 2.6               |
| 1%Pt/TiCD(20)             | 0.34    | 4.9          | 55.3                           | 123  | 3.2                | 8.8   | 2.8               |

<sup>a</sup> CD Maintained: (TMS-CD<sub>Catalyst</sub>/TMS-CD<sub>Support</sub>) × 100%.

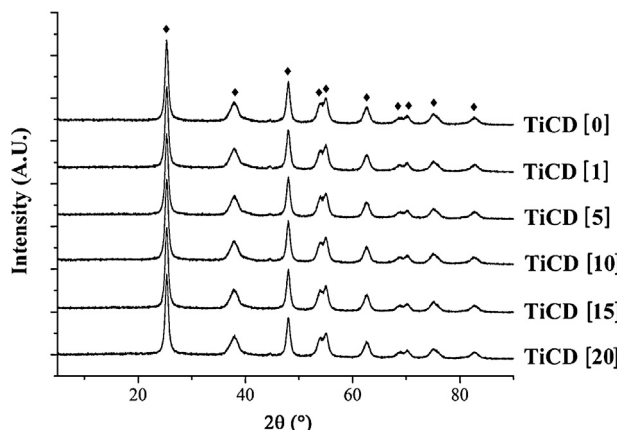


**Fig. 4.** XRD patterns of the catalysts synthesised on modified supports. ◆ corresponds to the anatase-TiO<sub>2</sub> phase (JCPDS 89-4921).

surface were identified as Pt particles. The average Pt particle size in **Table 2** is smaller than 3 nm for all the catalysts. The size of Pt particles on TiCD[ $x$ ] displayed a similar distribution size, independent of the TMS-CD content, which differs from the results recorded using Al<sub>2</sub>O<sub>3</sub> and SiO<sub>2</sub> materials [20,21]. The stoichiometric addition of NaOH during the Pt nanoparticles synthesis allowed for a basic medium during the reduction process. In this case, TiO<sub>2</sub> was activated using an aprotic solvent medium to improve hydroxyl formation and to avoid Ti-OH alkoxylation with protic solvent [30,31]. These hydroxyl groups enhance the metal retention on the TiO<sub>2</sub> surface for complexing with the PtCl<sub>6</sub><sup>2-</sup> metal precursor. In this case, the supports were contacted with a precursor solution at pH ~ 2.7. This phenomenon may be rationalised in terms of the surface properties of TiO<sub>2</sub> and the hydrolytic behaviour of PtCl<sub>6</sub><sup>2-</sup> in aqueous solution. In the case of TiO<sub>2</sub>-anatase, the zero point charge (pH zpc) is 6.25 [32]. Hence, at more acidic pH values, the surface is positively charged, whereas at pH values above 6.25, it is negatively charged [33]. In an aqueous solution, PtCl<sub>6</sub><sup>2-</sup> undergoes a

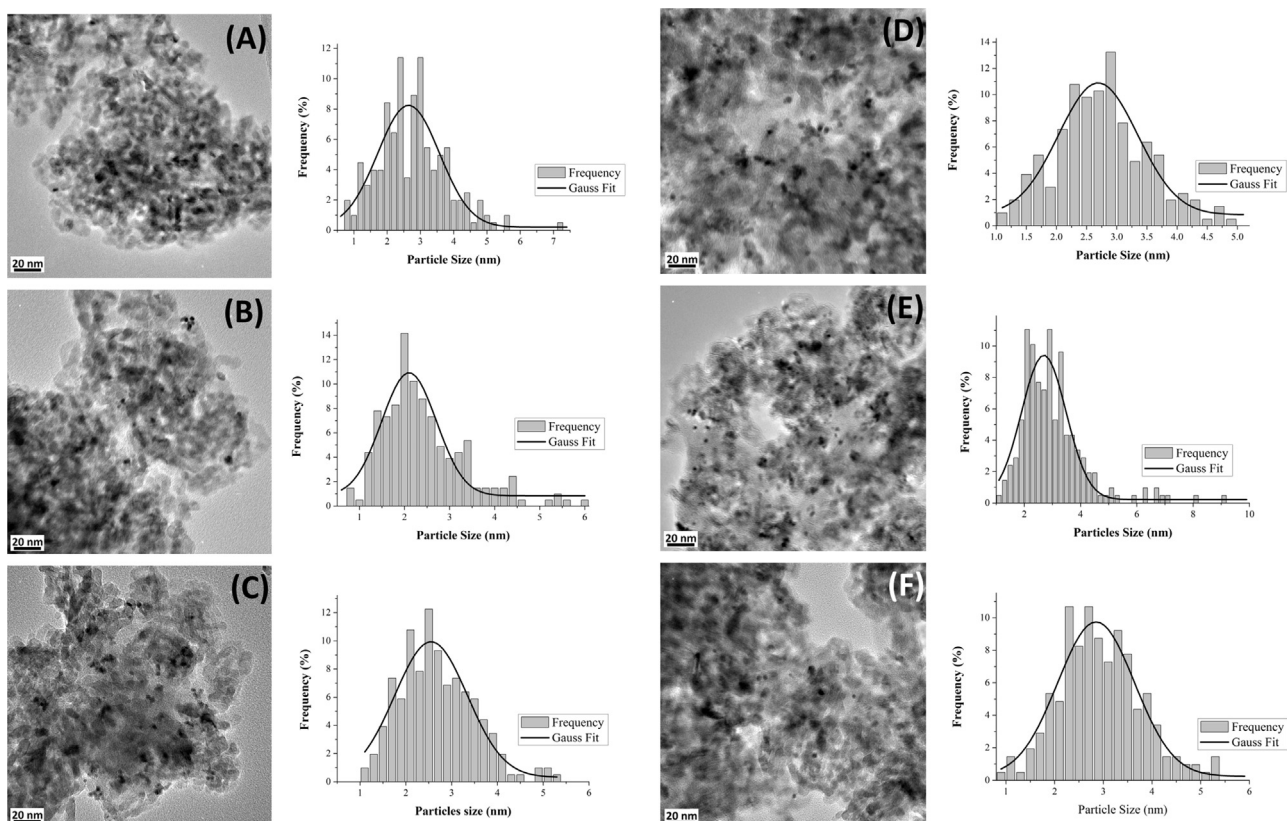
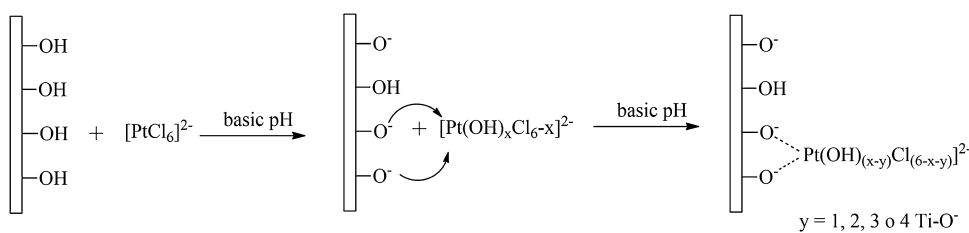
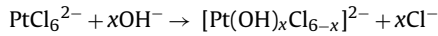


**Fig. 5.** HR-TEM micrograph of the 1 wt%Pt catalysts supported on the modified anatase-TiO<sub>2</sub> (a) TiCD[0]; (b) TiCD[1]; (c) TiCD[5]; (d) TiCD[10]; (e) TiCD[15] and (f) TiCD[20].



**Scheme 3.** Schematic deposition of metal  $[PtCl_6]^{2-}$  complexes onto  $TiO_2$  surfaces.

sequential hydrolysis to give various hydrolytic products, as mentioned by some authors [34–36]:



Under a basic medium, the negatively charged surface of  $TiO_2$  would explain the anchoring behaviour of the platinum complex. The increase of pH allows the reaction of the  $PtCl_6^{2-}$  precursor to give mixed  $[PtCl_{6-x}(OH)_x]^{2-}$  species [36,37]. A series of ligand substitution reactions of  $[PtCl_6]^{2-}$  in aqueous hydroxide medium and, at the same time, the  $TiO_2$  surface change, result in anionic species, such as  $Ti-O^-$ . This charged oxygen is basic and allows the substitution of the  $OH^-$  groups from the  $[PtCl_{6-x}(OH)_x]^{2-}$  complex for  $Ti-O^-$  [37–39], as shown in Scheme 3. However, during the precursor reduction, the  $H_2$  is consumed and consequently leads to a decrease of the pH. This is the reason for using  $Pt:OH = 6$  or a stoichiometric quantity of hydroxyl groups to give a pH neutral solution.

On a negatively charged surface of  $TiO_2$ , the concentration of  $[Pt(OH)_xCl_{6-x}]^{2-}$ -hydrolysed products is expected to be adsorbed on the surface by the  $Ti-O$ -complex bond, which in turn leads to a fast deposition rate that results in a smaller size of platinum particles. In alkaline reduction conditions ( $pH \geq 9$ ), the shape of the Pt nanoparticles appeared spherical, and the agglomeration of platinum was not observed. The catalyst prepared on the activated support ( $TiCD[0]$ ) displayed small particle sizes, reaching approximately 2.6 nm, and a narrow distribution of particle size values. The organic molecule does not influence the Pt cluster formed during the metal reduction. Given these conditions of catalyst preparation, a random deposition towards immobilised TMS-CD sites was expected.

The oxidation states of the species on the catalysts surface were investigated by XPS. Table 3 compiles the Pt 4f<sub>7/2</sub>, N 1s, O 1s and Ti 2p<sub>3/2</sub> binding energies (BE) for all the catalysts under study with the corresponding contribution to the overall signal in parentheses. The Pt 4f spectra of the  $Pt/TiCD[x]$  catalysts showed only one doublet, with the most intense Pt4f<sub>7/2</sub> component placed at 73.3–73.5 eV. After precursor reduction in  $H_2$  at room temperature and 40 bar, the metallic clusters displayed small particle sizes. The electronic properties of these very small Pt clusters on  $TiO_2$  regularly displayed a convolution of mainly  $Pt^0$  and  $Pt^{\delta+}$  (where  $0 < \delta < 1$ ) species [40,41];

for larger sized Pt clusters, the contribution of  $Pt^{\delta+}$  species was more significant [42]. The Pt 4f<sub>7/2</sub> BE appears at ~73.5 eV. This value is close to that reported by Huang et al. for similar  $TiO_2$ -supported Pt particles and corresponds to a negative shift of ~0.2 eV compared to the most common value measured for bulk  $Pt^0$  at 73.7 eV [41,43]. Such negative shifts can be explained by strong support-metal interactions. Charge transfer from the support to the particle, especially in systems with metallic particles on reducible metal oxides, can alter the electronic properties of the particle [44]. Small particles also have a large number of surface atoms with reduced coordination number. This feature is known to induce negative binding energy shifts relative to the value measured for the bulk metal [45]. The main  $\Delta BE$  to Pt peak (4f<sub>7/2</sub>) detected for the catalyst supports on  $TiCD[x]$  with  $[x] > 0$  showed a major decrease for the peak positions, compared to those for bulk Pt (~0.4–0.5 eV), suggesting that the Pt clusters are negatively charged because of the electron-donating nature of TMS-CD on the surface. A similar behaviour has been reported for Pt-PVP stabilised nanoparticles [46]. Conversely to our previously reported results for  $SiO_2$  and  $\gamma-Al_2O_3$  [20,21],  $TiO_2$ -anatase modified catalysts showed negatively charged Pt clusters, and an increase of TMS-CD on the support surface provide an electronic variation of Pt species.

The N 1s is another important signal in determining the nature of TMS-CD on the surface. For aromatic sp<sup>2</sup> or aliphatic sp<sup>3</sup>-hybridised nitrogen ( $N_{\text{neutral}}$ ), characteristic peaks at 399.0–399.8 eV were found [47]. In our case, two contributions for N 1s peak were detected at 399.8–399.9 and 401.3–401.6 eV. The first corresponds to  $N_{\text{neutral}}$  typical for non-adsorbed TMS-CD molecules [48,49]. The second can be attributed to positively charged nitrogen ( $N_{\text{ionic}}$ ), in agreement with previous results reported by Bonello et al. [50] and Evans et al. [51]. The  $N_{\text{neutral}}$  and  $N_{\text{ionic}}$  signals correspond to both nitrogen atoms from TMS-CD, and these were not resolved so that only an average value was determined. In addition, the chemical shift for the second  $N_{\text{ionic}}$  signals can be attributed to the  $Ti-OH$  surface interaction with quinuclidinic and quinolinic N atoms due to an acid–base effect induced by H bond formation (see Table 3). In previous works,  $SiO_2$  and  $\gamma-Al_2O_3$  oxides were used as supports for the immobilisation of TMS-CD and Pt deposition by the same synthetic routes. In both supports, a different BE for N 1s was detected [20,21]. Fig. 6 displays a comparison of  $\Delta BE$  for the N 1s

**Table 3**  
Binding energies (eV) of internal electrons and atomic surface ratio of 1 wt%Pt/ $TiCD(x)$  catalysts.

| Catalyst         | Pt 4f <sub>7/2</sub> (eV) | N 1s (eV)  | Ti 2p <sub>3/2</sub> (eV) | O 1s                     | Pt/Ti at | N/Ti at |
|------------------|---------------------------|------------|---------------------------|--------------------------|----------|---------|
| 1%Pt/ $TiCD(0)$  | 73.6                      | –          | 458.6                     | 529.9 (79)<br>531.5 (21) | 0.0030   | –       |
| 1%Pt/ $TiCD(1)$  | 73.4                      | 399.7 (82) | 458.6                     | 530.0 (84)               | 0.0046   | 0.035   |
|                  |                           | 401.5 (18) |                           | 531.6 (16)               |          |         |
| 1%Pt/ $TiCD(5)$  | 73.3                      | 399.8 (75) | 458.6                     | 530.0 (84)               | 0.0045   | 0.048   |
|                  |                           | 401.5 (25) |                           | 531.5 (16)               |          |         |
| 1%Pt/ $TiCD(10)$ | 73.3                      | 399.8 (73) | 458.6                     | 530.0 (84)               | 0.0060   | 0.053   |
|                  |                           | 401.4 (27) |                           | 531.6 (16)               |          |         |
| 1%Pt/ $TiCD(15)$ | 73.3                      | 399.8 (73) | 458.6                     | 529.9 (84)               | 0.0088   | 0.067   |
|                  |                           | 401.3 (27) |                           | 531.5 (16)               |          |         |
| 1%Pt/ $TiCD(20)$ | 73.3                      | 399.9 (71) | 458.6                     | 529.9 (83)               | 0.0079   | 0.077   |
|                  |                           | 401.4 (29) |                           | 531.5 (17)               |          |         |

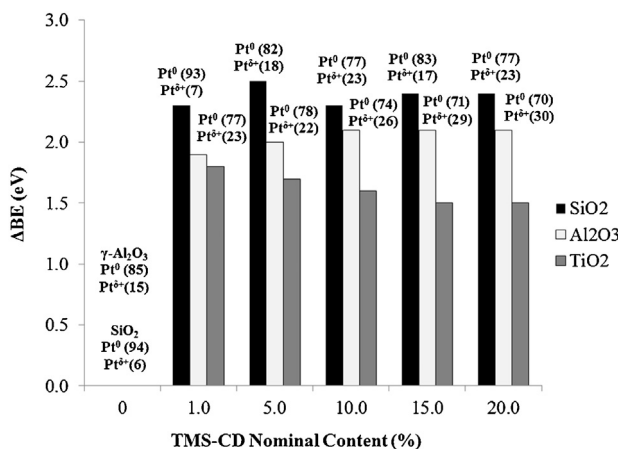


**Fig. 6.** ΔBE for the N 1s determinate by XPS for different TMS-CD wt% anchored on different supports. The data for the SiO<sub>2</sub> and γ-Al<sub>2</sub>O<sub>3</sub> supports was extracted from [20] and [21], respectively. Percentage contributions to the Pt overall signal in parentheses.

obtained in these three different supports. The SiO<sub>2</sub> modified supports show a constant ΔBE attributed to the retro-donation effect from TMS-CD to Pt nanoparticles because, in absence of TMS-CD, the catalyst shows 9% Pt<sup>δ+</sup> on the surface, and with the increase of the immobilised-modifier content, an increment of Pt<sup>δ+</sup> species was detected. The γ-Al<sub>2</sub>O<sub>3</sub> modified supports showed a different trend. These catalysts displayed a strong Pt–Al<sub>2</sub>O<sub>3</sub> interaction, which provides more positively charged Pt clusters (15% Pt<sup>δ+</sup> contribution on γ-Al<sub>2</sub>O<sub>3</sub> without TMS-CD). This interaction increases with the increase of the TMS-CD content because the modifier molecules cover the support surface; this coverage promotes the effective interaction between N atoms and Pt clusters. Both supports displayed a decrease in the Pt nanoparticles size distribution with the increase of TMS-CD, in agreement with the strong interaction detected by XPS [45]. In TiO<sub>2</sub> supports, a decrease of ΔBE was detected with the increase of TMS-CD on the support surface. In these catalysts, convolution of the Pt<sup>0</sup>/Pt<sup>δ+</sup> contribution in Pt 4f<sub>7/2</sub> signals was not detected because the strong metal support interaction provides negatively charged Pt nanoparticles. The active phase did not show a TMS-CD–Platinum retrodonation, and the N<sub>ionic</sub> species contribution could only correspond to inducer-TiO<sub>2</sub> acid–basic interaction. This is in agreement with the decrease of ΔBE in the TiO<sub>2</sub> catalyst because the TMS-CD surface coverage decreases the direct interaction between Ti–OH and N atoms by Ti–O–Si bond formation. In addition, the metal particle size distributions did not show a variation with the TMS-CD content on surface, as shown by HR-TEM.

However, at higher TMS-CD contents, the surface Pt/Ti atomic ratio increased, and the entire N/Ti atomic ratio showed a higher value in relation with the bulk atomic ratios, as shown in Table 3, mainly due to the surface coverage of the TMS-CD on the TiO<sub>2</sub>-anatase support.

### 3.3. Enantioselective hydrogenation of PPD

#### 3.3.1. TMS-CD Effect

We initially investigated the influence of the TMS-CD amount on the catalytic performance in the asymmetric hydrogenation of PPD with Pt/TiCD[x] catalysts and evaluated the optimal concentration of TMS-CD. Fig. 7 shows the profiles of conversion vs. time in PPD hydrogenation. A pseudo-first-order kinetics with respect to PPD was found in all cases, reaching conversion levels over 85% at 240 min of reaction for the 1%Pt/TiCD[x] with 0 < [x] < 5 and under 80% for those with [x] < 5. Scheme 2 depicts the hydrogenation reaction of the substrate only in

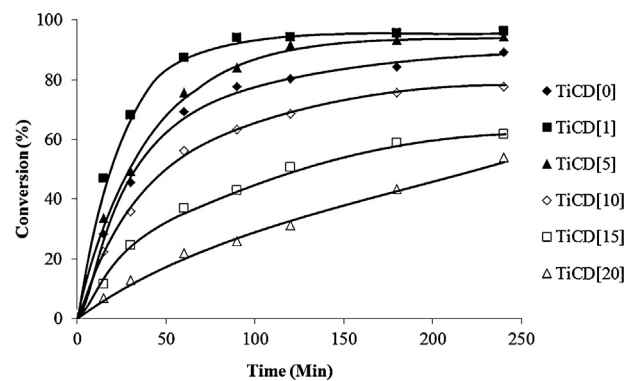


**Fig. 7.** Activity curves based on PPD conversion for 1%Pt/TiCD[x] catalysts. Reaction conditions: PPD concentration: 0.01 mol L<sup>-1</sup>, catalyst mass: 0.050 g, P<sub>H2</sub>: 40 bar, stirring speed: 700 rpm, solvent: cyclohexane.

relation to the carbonyl groups without consecutive hydrogenation to obtain di-hydroxylated products. All of the catalysts were enantioselective for (R)-1-hydroxy-1-phenylpropan-2-one (1R-PP) and (R)-2-hydroxy-1-phenylpropan-1-one (2R-PP), no other hydrogenated products were detected.

With respect to enantioselectivity, the reaction with activated and bare TiO<sub>2</sub> displayed the racemic mixtures, although the conversion reached 89%. On the catalysts supported on TiCD[x] with [x] > 0, an increase in the conversion to PPD was detected up to TiCD(5), reaching 95% of PPD conversion and suggesting that the hydrogenation was a “ligand-accelerated” reaction similar to previous studies reported by Margitfalvi et al. [52–54]. According to these authors, this feature can be explained by the formation of a weak modifier–substrate complex for the supported metallic catalysts where the inducer was added in situ. Table 4 shows the conversion levels and the pseudo-constant rate, k<sub>g</sub>. An increase of the TMS-CD content resulted in higher surface coverage, and the supported catalysts on TiCD[x] with [x] > 5 showed lower conversion levels. This suggests a change of the metallic site environment. However, these catalysts showed a regular and uniform metal size particle distribution, independent of the quantity of anchoring modifier on the surface. An increase of TMS-CD caused a decrease in the catalytic activity by surface blockage of the active sites by repulsive steric interactions with the immobilised inducer. This behaviour is similar to that previously reported by Toukoniitty et al. [8,10–12] and Reyes et al. [6,7,55,56] in the same reaction where the CD was added in situ.

Fig. 8 shows the evolution of the enantiomeric excess (ee) vs. conversion. All the catalysts were selective for the hydrogenation

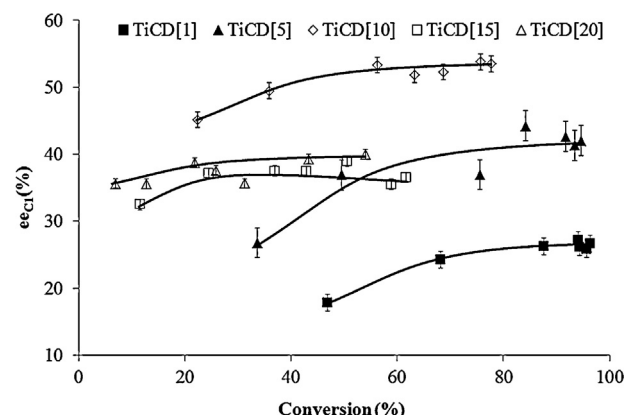


**Fig. 8.** Enantiomeric excess vs. PPD conversion for 1%Pt/TiCD[x] catalysts. Reaction conditions: PPD concentration: 0.01 mol L<sup>-1</sup>, catalyst mass: 0.050 g, P<sub>H2</sub>: 40 bar, stirring speed: 700 rpm, solvent: cyclohexane.

**Table 4**

Catalytic data for PPD hydrogenation over 1%Pt/TiCD(x) catalysts. Reaction conditions: PPD concentration: 0.01 mol L<sup>-1</sup>,  $P_{H_2}$ : 40 bar, catalyst mass: 0.050 g, stirring rate: 700 rpm, solvent: cyclohexane at 298 K.

| TMS-CD nominal (%) | Conversion <sup>a</sup> (%) | ee <sub>C1</sub> <sup>b</sup> (%) | ee <sub>C2</sub> <sup>b</sup> (%) | rs <sup>b</sup> | $k_g$ <sup>c</sup> (min <sup>-1</sup> g <sup>-1</sup> ) | $k_{1R}$ (min <sup>-1</sup> g <sup>-1</sup> ) | $k_{1S}$ (min <sup>-1</sup> g <sup>-1</sup> ) | $k_{2R}$ (min <sup>-1</sup> g <sup>-1</sup> ) | $k_{2S}$ (min <sup>-1</sup> g <sup>-1</sup> ) |
|--------------------|-----------------------------|-----------------------------------|-----------------------------------|-----------------|---|---|---|---|---|
| 0                  | 89.1                        | 0.4                               | 0.6                               | 62              | 0.358   | —   | —   | —   | —   |
| 1                  | 96.3                        | 24.9                              | 10.3                              | 62              | 0.642   | 0.422   | 0.199   | 0.012   | 0.010   |
| 5                  | 94.6                        | 38.7                              | 26.6                              | 49              | 0.428   | 0.271   | 0.114   | 0.028   | 0.016   |
| 10                 | 77.7                        | 51.4                              | —                                 | —               | 0.284   | 0.217   | 0.067   | —   | —   |
| 15                 | 61.7                        | 36.5                              | —                                 | —               | 0.128   | 0.088   | 0.040   | —   | —   |
| 20                 | 54.1                        | 37.5                              | —                                 | —               | 0.064   | 0.044   | 0.020   | —   | —   |

<sup>a</sup> 240 min of reaction.

<sup>b</sup> Average values.

<sup>c</sup>  $k_g = k_{1R} + k_{1S} + k_{2R} + k_{2S}$ .

**Table 5**

Catalytic data for PPD hydrogenation on 1%Pt/TiCD(10) catalyst at different H<sub>2</sub> pressures. Reaction conditions: PPD concentration: 0.01 mol L<sup>-1</sup>, catalyst mass: 0.050 g and stirring rate: 700 rpm, solvent: cyclohexane at 298 K.

| Pressure (bar) | Conversion <sup>a</sup> (%) | ee <sub>C1</sub> <sup>b</sup> (%) | $k_g$ <sup>c</sup> (min <sup>-1</sup> g <sup>-1</sup> ) | $k_{1R}$ (min <sup>-1</sup> g <sup>-1</sup> ) | $k_{1S}$ (min <sup>-1</sup> g <sup>-1</sup> ) |
|----------------|-----------------------------|-----------------------------------|---|---|---|
| 20             | 64.4                        | 47.3                              | 0.172   | 0.127   | 0.045   |
| 40             | 77.7                        | 51.4                              | 0.284   | 0.217   | 0.067   |
| 60             | 90.7                        | 51.3                              | 0.382   | 0.289   | 0.093   |
| 80             | 91.8                        | 52.0                              | 0.508   | 0.386   | 0.122   |

<sup>a</sup> 240 min. of reaction.

<sup>b</sup> Average values.

<sup>c</sup>  $k_g = k_{1R} + k_{1S}$ .

of the carbonyl groups (see Scheme 2). 1R-PP was the main reaction product, and the ee<sub>C1</sub> was similar to those reported for systems in which the chiral inducer was added in situ and adsorbed on the surface of the catalyst [55,56]. When increasing the TMS-CD amount on the TiO<sub>2</sub> surface, the ee was further improved to a maximum of 51% for the catalyst 1%Pt/TiCD(10). At higher TMS-CD contents, the conversion and ee value decreased.

The most active catalysts (TiCD[x] with [x] < 10) showed hydrogenation of the carbonyl of the acetyl group (C2), with 2R-PP being the preferred product. All these supports show a low loading of TMS-CD (see Table 2) and possess different type of acid-base sites: Ti<sup>4+</sup> (Lewis acid) and O<sup>2-</sup> (Lewis base) ions [28]. The acid sites can promote the hydrogenation of non-planar groups by interactions with the non-bonding electrons from the carbonyl groups. The Lewis acid Ti<sup>4+</sup> centres exposed at the surface can interact with the carbonyl of the acetyl group through linear adsorption and decrease the ability of parallel adsorption by steric hindrance of the methyl group, decreasing the effective formation of modifier–substrate complexes over metallic modified sites and, consequently, the enantioselection capacity.

The rs values showed a high hydrogenation rate of the carbonyl adjacent to the phenyl group (C1), with values of 67 for the catalyst 1% Pt/TiCD(0). This is due to the high adsorption capacity of the phenyl group of PPD at the active sites (for  $\eta$  bond formation between the active phase and the  $\pi$  aromatic cloud of the phenyl group), in line with studies by Toukoniitty et al. [8,10–12]. Pt nanoparticles are negatively charged, and this property could enhance the regioselectivity.

### 3.3.2. Effect of H<sub>2</sub> pressure

After finding the most enantioselective catalytic system, i.e., Pt/TiCD(10), the effect of H<sub>2</sub> pressure over the PPD hydrogenation was studied, and the results are shown in Table 5. The surface H<sub>2</sub> concentration may directly influence the adsorption of the reactant and thus, the enantioselectivity. An H<sub>2</sub> pressure increase (from 20 to 80 bar) had a marked effect on the conversion levels but only a discreet effect on the ee<sub>C1</sub> value. The best ee<sub>C1</sub> value was achieved at 40 bar, similarly to that previously reported [20,21].

### 3.3.3. Effect of PPD concentration

The enantioselective 1%Pt/TiCD(10) catalysed hydrogenation reaction was performed with different PPD initial concentrations.

Increasing the liquid phase substrate concentrations led to a significant effect on the catalytic behaviour. Table 6 shows the kinetic results for all the used concentrations. The conversion and ee decreased with increasing substrate/metal molar ratio while keeping the catalyst mass constant. The conversion decreased drastically with further increase in the PPD concentration, whereas a different trend in the ee was detected. For all the PPD concentrations, the reaction only showed hydrogenation of C1, but the substrate/metal mole ratio affect the enantioselectivity of this catalyst. At lower concentrations of PPD, the Pt nanoparticles on the surface located on unattached TMS-CD sites are the most available for the adsorption of PPD and give racemic mixtures. In contrast, at higher PPD concentrations the amount of substrate on the Pt surface should increase. The mechanistic studies reported by Toukoniitty et al. [10,12] demonstrated the influence on the parallel adsorption of phenyl groups on Pt clusters controls the ee. When the PPD concentration increases, different adsorption modes can occur on the Pt clusters and provide non-enantioenriched mixtures.

### 3.3.4. Effect of the solvent

In heterogeneous asymmetric hydrogenation, the enantioselectivity is very sensitive to the solvent used, and some examples of this effect can be found in literature for the hydrogenation of PPD catalysed by Pt-CD [21,52,57,58]. The effect of solvents with dielectric constants ranging from 2 to 25 (values of pure solvents) have been included in this study for the hydrogenation of PPD catalysed by 1%Pt/TiCD(10). The results are displayed in Fig. 9 and correspond to a qualitative model including the enantioselectivity and the dielectric constant of the pure solvents, similar to that proposed by Toukoniitty et al. [58]. The highest activity was observed in ethyl acetate, and very low reaction rates were obtained in tetrahydrofuran, whereas relatively high rates were obtained in the other solvents in this study. Toukoniitty et al. [58] reported that the initial hydrogenation rate does not correlate with the hydrogen solubility. In terms of enantioselectivity, among the solvents investigated, cyclohexane led to the best e.e. values of 51% at 78% of conversion. Conversely to previous reported results for TMS-CD- $\gamma$ -Al<sub>2</sub>O<sub>3</sub> supports, toluene showed a lower reaction rate in comparison to cyclohexane [21]. Both solvents have similar dielectric constants and have shown high conversion and ee in PPD hydrogenation using the same reaction conditions [21]. In our case, the electronic

**Table 6**

Catalytic data for PPD hydrogenation on 1%Pt/TiCD(10) catalyst at different PPD concentrations. Reaction conditions:  $P_{\text{H}_2}$ : 40 bar, catalyst mass: 0.050 g and stirring rate: 700 rpm, solvent: cyclohexane at 298 K.

| Concentration (mol L <sup>-1</sup> ) | Mole ratio PPD/Pt <sub>total</sub> | Conversion <sup>a</sup> (%) | ee <sub>C1</sub> <sup>b</sup> (%) | $k_g$ <sup>c</sup> (min <sup>-1</sup> g <sup>-1</sup> ) | $k_{1R}$ (min <sup>-1</sup> g <sup>-1</sup> ) | $k_{1S}$ (min <sup>-1</sup> g <sup>-1</sup> ) |
|--------------------------------------|------------------------------------|-----------------------------|-----------------------------------|---|---|---|
| 0.005                                | 25                                 | 94.5                        | 38.7                              | 0.412   | 0.299   | 0.113   |
| 0.010                                | 50                                 | 77.7                        | 51.4                              | 0.284   | 0.217   | 0.067   |
| 0.025                                | 125                                | 68.7                        | 47.6                              | 0.172   | 0.129   | 0.043   |
| 0.100                                | 500                                | 51.3                        | 43.4                              | 0.08  | 0.058   | 0.022   |

<sup>a</sup> 240 min of reaction.

<sup>b</sup> Average values.

<sup>c</sup>  $k_g = k_{1R} + k_{1S}$ .

**Table 7**

EA, HR-TEM mean Pt sizes and XPS data for recycles of the catalyst 1%Pt/TiCD(10). Reaction conditions: PPD concentration: 0.01 mol L<sup>-1</sup>, catalyst mass: 0.070 g per cycle,  $P_{\text{H}_2}$ : 40 bar, stirring rate: 700 rpm at 298 K.

| Cycle | N(%) <sup>a</sup> | TMS-CD (wt %) | Pt 4f <sub>7/2</sub> (eV) | N1s (eV)                 | Pt/Ti at | N/Ti at | $d_p$ HR-TEM <sup>b</sup> (nm) |
|-------|-------------------|---------------|---------------------------|--------------------------|----------|---------|--------------------------------|
| Fresh | 0.22              | 3.2           | 73.3                      | 399.8 (73)<br>401.3 (27) | 0.0060   | 0.053   | 2.6                            |
| 1     | 0.22              | 3.2           | 73.3                      | 399.9 (74)<br>401.3 (26) | 0.0056   | 0.057   | –                              |
| 2     | 0.22              | 3.1           | 73.4                      | 400.0 (75)<br>401.3 (25) | 0.0064   | 0.063   | –                              |
| 3     | 0.22              | 3.2           | 73.3                      | 400.0 (75)<br>401.4 (25) | 0.0058   | 0.058   | –                              |
| 4     | 0.22              | 3.1           | 73.4                      | 400.1 (76)<br>401.4 (23) | 0.0062   | 0.052   | –                              |
| Final | 0.22              | 3.1           | 73.4                      | 400.1 (76)<br>401.4 (23) | 0.0049   | 0.055   | 2.5                            |

<sup>a</sup> Average value from two measurements.

<sup>b</sup> Only to fresh catalyst and after the last run was measured.

nature of Pt nanoparticles provided a competition between PPD and toluene for  $\eta$  bond interactions formation on the active phase surface ( $\pi$  aromatic bonds), decreasing the conversion levels and ee. The ee was almost 34% in ethanol and decreased to 22% in toluene. Finally, ee decreased non-linearly with increasing solvent dielectric constant, which was attributed to the interactions between solvents and TMS-CD on the surface. On the other hand, these results do not show a clear correlation between the catalytic performance and solvent polarity, in agreement with similar studies reported by Toukoniity et al. for commercial Pt, Pd and Rh/ $\gamma$ -Al<sub>2</sub>O<sub>3</sub> supported catalysts [8].

### 3.3.5. Recycling

The catalyst 1%Pt/TiCD(10) catalyst was used to perform recycling studies. Between cycles, the catalyst was washed with

chloroform to remove the organic matter that could have been adsorbed on the support and the TMS-CD from leaching [59]. Fig. 10 shows the variation of the conversion and ee levels as a function of the number of reaction cycles. All the cycles show a pseudo-first-order trend during the hydrogenation reaction. As the number of reaction runs increased, the activity decreased, reaching values of 30% in the last cycle.

Table 7 shows the catalyst characterisation after each cycle. N(%) shows constants values during the cycles, suggesting that non-leaching of the inducer was detected. The active phase showed constant values for the Pt BE and Pt/Ti surface atomic ratios after all the cycles. The nanoparticle distribution sizes displayed a similar trend and regular shapes as fresh 1%Pt/TiCD(10) catalyst. For both reasons, non-leaching and/or sintering of nanoparticles was assumed in all runs. The XPS shows the presence of two types of surface nitrogen, N<sub>neutral</sub> and N<sub>ionic</sub>, as was discussed in previous sections. The remaining anchored chiral inducer is slightly

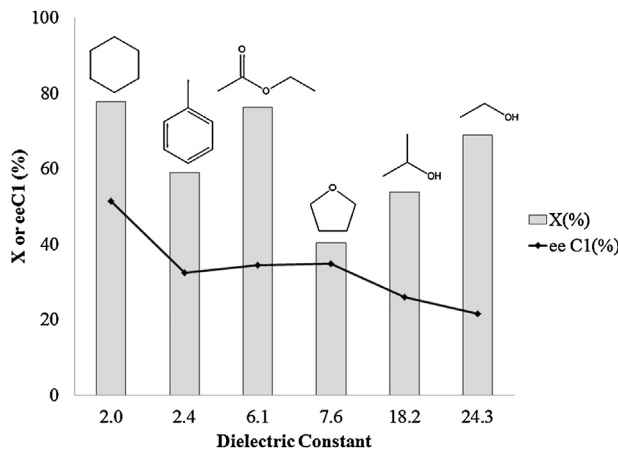


**Fig. 9.** Curves of the enantiomeric excess and PPD conversion vs. dielectric constant for PPD hydrogenation on 1%Pt/TiCD[10] at different solvents. Reaction conditions: PPD concentration 0.01 mol L<sup>-1</sup>,  $P_{\text{H}_2}$ : 40 bar, catalyst mass: 0.050 g and stirring speed: 700 rpm.

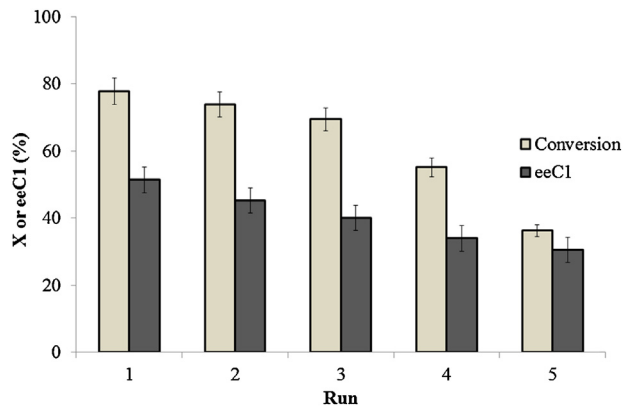


**Fig. 10.** Activity and ee as a function of the number of reaction cycles for the catalyst 1%Pt/TiCD[10]. Reaction conditions: PPD concentration: 0.01 mol L<sup>-1</sup>, catalyst mass: 0.070 g,  $P_{\text{H}_2}$ : 40 bar, stirring speed: 700 rpm, solvent: cyclohexane.

hydrogenated in the quinoline cycle of the TMS-CD because a slight N<sub>neutral</sub> BE shift to a higher value was detected. The N 1s for aliphatic N (piperidine contribution) at 400.0 eV has been reported by Luo et al. [60,61]. These N 1s BE values are in agreement with N<sub>neutral</sub> and N<sub>ionic</sub> contributions because in all the cycles, these values were constant. For quinoline hydrogenation, in the absence of leaching, the contribution of ionic species should not increase. TMS-CD hydrogenation on the support led to lower activity because they might be interfering with the adsorption of the substrate on the active sites. Subsequently, this blockage poisons the active sites close to the modified sites, and the hydrogenation only takes place on the unmodified Pt nanoparticles. Consequently, the reaction on these sites leads to a racemic mixture and thus decreasing ee values.

#### 4. Conclusions

New catalyst systems were synthesised for the enantioselective hydrogenation of PPD. Cinchonidine was tethered directly with prior silanisation modification over activated anatase-TiO<sub>2</sub>. The supported metallic catalysts were obtained by the reduction of a metallic precursor under high H<sub>2</sub> pressure. The characterisation data provide evidence of the immobilisation of cinchonidine. The HR-TEM images and XPS demonstrated that the cinchonidine content does not affect the active phase dispersion and particle size distribution. It can be deduced from the XPS results that the Pt nanoparticles exhibited a negative charged surface, which was attributed to the metal deposition method and the strong interaction with the TiO<sub>2</sub> surface. The 1% Pt/TiCD[x] catalysts displayed relatively high conversion and ee values (51.0%). The catalyst with [x]=10 presented performances similar to those previously reported for a commercial Pt/Al<sub>2</sub>O<sub>3</sub> catalyst, where untethered cinchonidine was used. The effect of the H<sub>2</sub> pressure, PPD concentration in the liquid phase and solvents indicated that the reaction conditions were important in controlling the activity and enantioselectivity. This is explained by the substrate adsorption on the Pt sites. The solvent effect studies showed non-linear correlation between enantiomeric excess and the dielectric constant of the pure solvent. The most selective catalyst showed good reusability under optimum conditions and deactivation by hydrogenation of TMS-CD after the third cycle.

#### Acknowledgements

The authors thank CONICYT for the financial support (FONDECYT GRANT 1061001, FONDECYT Initiation GRANT 11121631, FONDECYT postdoctoral 3130483) and REDOC.CTA doctoral network.

#### References

- [1] H.-U. Blaser, F. Spindler, M. Studer, *Appl. Catal. A: Gen.* 221 (2001) 119–143.
- [2] T. Katsuki, *Comprehensive Asymmetric Catalysis*, Berlin, 1999.
- [3] D. Pauluth, A.E.F. Wachter, *Chirality in Industry II*, 1997.
- [4] M. Studer, H.-U. Blaser, C. Exner, *Adv. Synth. Catal.* 345 (2003) 45–65.
- [5] W.A.H. Vermeer, A. Fulford, P. Johnston, P.B. Wells, *J. Chem. Soc. Chem. Commun.* (1993) 1053–1054.
- [6] N.M. Marin, G. Pecchi, P. Reyes, *React. Kinet. Catal. Lett.* 87 (2006) 121–128.
- [7] T. Marzialetti, J.L.G. Fierro, P. Reyes, *Catal. Today* 107–108 (2005) 235–243.
- [8] E. Toukoniitty, S. Franceschini, A. Vaccari, D.Y. Murzin, *Appl. Catal. A: Gen.* 300 (2006) 147–154.
- [9] E. Toukoniitty, P. Mäki-Arvela, N. Kumar, T. Salmi, D.Y. Murzin, *Catal. Today* 79–80 (2003) 189–193.
- [10] E. Toukoniitty, P. Mäki-Arvela, J. Wärnå, T. Salmi, *Catal. Today* 66 (2001) 411–417.
- [11] E. Toukoniitty, V. Nieminen, A. Taskinen, J. Pääväranta, M. Hotokka, D.Y. Murzin, *J. Catal.* 224 (2004) 326–339.
- [12] E. Toukoniitty, B. Ševčíková, P. Mäki-Arvela, J. Wärnå, T. Salmi, D.Y. Murzin, *J. Catal.* 213 (2003) 7–16.
- [13] V.B. Shukla, P.R. Kulkarni, *World J. Microbiol. Biotechnol.* 16 (2000) 499.
- [14] A. Ghosh, R. Kumar, *J. Catal.* 228 (2004) 386–396.
- [15] D. Ruiz, C. Mella, P. Reyes, J.L.G. Fierro, *J. Chil. Chem. Soc.* 57 (2012) 1394–1399.
- [16] D. Ruiz, M. Oportus, C. Godard, C. Claver, J.L.G. Fierro, P. Reyes, *Curr. Org. Chem.* 16 (2012) 2754–2762.
- [17] C.E. Song, S.-G. Lee, *Chem. Rev.* 102 (2002) 3495–3524.
- [18] D.D. Vos, I.F.J. Vankelecom, P.A. Jacobs, *Chiral Catalyst Immobilization and Recycling*, Toronto, 2000.
- [19] M.U. Azmat, Y. Guo, Y. Guo, Y. Wang, G. Lu, *J. Mol. Catal. A: Chem.* 336 (2011) 42–50.
- [20] C.H. Campos, M. Oportus, C. Torres, C. Urbina, J.L.G. Fierro, P. Reyes, *J. Mol. Catal. A: Chem.* 348 (2010) 30–41.
- [21] C.H. Campos, C. Torres, J.L.G. Fierro, P. Reyes, *Appl. Catal. A: Gen.* 466 (2013) 198–207.
- [22] D. Ruiz, J.L.F. Fierro, P. Reyes, *J. Braz. Chem. Soc.* 21 (2010) 262–269.
- [23] D. Ruiz, P. Reyes, *J. Chil. Chem. Soc.* 54 (2008) 1740–1742.
- [24] A. Lindholm, P. Mäki-Arvela, E. Toukoniitty, T.A. Pakkanen, T.J. Hirvi, T. Salmi, D.Y. Murzin, R. Sjöholm, R. Leino, *J. Chem. Soc. Perkin 1* 12 (2002) 2605.
- [25] E. Toukoniitty, P. Mäki-Arvela, A.K. Neyestanaki, T. Salmi, R. Sjöholm, R. Leino, E. Laine, P.J. Kooyman, T. Ollonqvist, J. Väyrynen, *Appl. Catal. A: Gen.* 216 (2001) 73–83.
- [26] C.D. Wagner, L.E. Davis, M.V. Zeller, J.A. Taylor, R.H. Raymond, L.H. Gale, *Surf. Interface Anal.* 3 (1981) 211–225.
- [27] V. Nieminen, A. Taskinen, M. Hotokka, D.Y. Murzin, *J. Catal.* 245 (2007) 228–236.
- [28] G. Martra, *App. Catal. A: Gen.* 200 (2000) 275–285.
- [29] K.S.W. Sing, *Pure Appl. Chem.* 54 (1982) 2201–2218.
- [30] J. Blümel, *J. Am. Chem. Soc.* 117 (1995) 2112–2113.
- [31] C.-H. Chu, E. Jonsson, M. Auvinen, J.J. Pesek, J.E. Sandoval, *Anal. Chem.* 65 (1993) 808–816.
- [32] G.A. Parks, *Chem. Rev.* 65 (1965) 177–198.
- [33] M. Muneer, M. Qamar, M. Saquib, D.W. Bahnemann, *Chemosphere* 61 (2005) 457–468.
- [34] L.E. Cox, D.G. Peters, E.L. Wehry, *J. Inorg. Nucl. Chem.* 34 (1972) 297–305.
- [35] Z. Jin, Z. Chen, Q. Li, C. Xi, X. Zheng, *J. Photochem. Photobiol. A: Gen.* 81 (1994) 177–182.
- [36] W.A. Speiker, J. Liu, J.T. Miller, A.J. Kropf, J.R. Regalbuto, *Appl. Catal. A: Gen.* 232 (2002) 219–235.
- [37] W.A. Speiker, J. Liu, X. Hao, J.T. Miller, A.J. Kropf, J.R. Regalbuto, *Appl. Catal. A: Gen.* 243 (2003) 53–66.
- [38] O.B. Bel'skaya, R.K. Karyanova, D.I. Kochubey, V.K. Duplyakin, *Kinet. Catal.* 49 (2008) 720–728.
- [39] B. Shelimov, J.-F. Lambert, M. Che, B. Didillon, *J. Catal.* 185 (1999) 462–478.
- [40] S.-H. Chien, M.-C. Kuo, C.-H. Lu, K.-N. Lu, *Catal. Today* 97 (2004) 121–127.
- [41] B.-S. Huang, F.-Y. Chang, M.-Y. Wey, *Int. J. Hydrogen Energy* 35 (2010) 7699–7705.
- [42] J. Croy, S. Mostafa, J. Liu, Y.-h. Sohn, B. Roldan Cuanya, *Catal. Lett.* 118 (2007) 1–7.
- [43] J.L.G. Fierro, J.M. Palacios, F. Tomas, *Surf. Interface Anal.* 13 (1988) 25–32.
- [44] S. Laursen, S. Linic, *Phys. Rev. Lett.* 97 (2006) 026101.
- [45] O. Björneholm, F. Federmann, F. Fössing, T. Möller, *Phys. Rev. Lett.* 74 (1995) 3017–3020.
- [46] M.J. Hossain, H. Tsunoyama, M. Yamauchi, N. Ichikuni, T. Tsukuda, *Catal. Today* 183 (2012) 101–107.
- [47] J.F. Moulder, W.F. Stickle, P.E. Sobol, K.D. Bomben, *Handbook of X-ray Photoelectron Spectroscopy*, Eden Prairie, 1995.
- [48] J.M. Bonello, R.M. Lambert, *Surf. Sci.* 498 (2002) 212–228.
- [49] A.F. Carley, M.K. Rajumon, M.W. Roberts, P.B. Wells, *J. Chem. Soc. Faraday Trans.* 91 (1995) 2167–2172.
- [50] J.M. Bonello, F.J. Williams, R.M. Lambert, *J. Am. Chem. Soc.* 125 (2003) 2723–2729.
- [51] T. Evans, A.P. Woodhead, A. Gutiérrez-Sosa, G. Thornton, T.J. Hall, A.A. Davis, N.A. Young, P.B. Wells, R.J. Oldman, O. Plashkevych, O. Vahtras, H. Ågren, V. Caravetta, *Surf. Sci.* 436 (1999) L691–L696.
- [52] J.L. Margitfalvi, E. Tálás, *App. Catal. A: Gen.* 301 (2006) 187–195.
- [53] J.L. Margitfalvi, E. Tálás, E. Tifirst, C.V. Kumar, A. Gergely, *Appl. Catal. A: Gen.* 191 (2000) 177–191.
- [54] J.L. Margitfalvi, E. Tifirst, *J. Mol. Catal. A: Chem.* 139 (1999) 81–95.
- [55] T. Marzialetti, M. Oportus, D. Ruiz, J.L.G. Fierro, P. Reyes, *Catal. Today* 133–135 (2008) 711–719.
- [56] C. Urbina, C.H. Campos, P. Reyes, P. Pecchi, *J. Chil. Chem. Soc.* 54 (2010) 331–336.
- [57] B. Toukoniitty, E. Toukoniitty, P. Mäki-Arvela, J.-P. Mikkola, T. Salmi, D.Y. Murzin, P.J. Kooyman, *Ultrasound Sonochem.* 13 (2006) 68–75.
- [58] E. Toukoniitty, P. Mäki-Arvela, J. Kuusisto, V. Nieminen, *J. Mol. Catal. A: Chem.* 192 (2003) 135–151.
- [59] A. Vargas, T. Bürgi, A. Baiker, *J. Catal.* 226 (2004) 69–82.
- [60] X. Luo, S.H. Goh, S.Y. Lee, *Macromolecules* 30 (1997) 4934–4938.
- [61] X. Luo, S.H. Goh, S.Y. Lee, K.L. Tan, *Macromolecules* 31 (1998) 3251–3254.